

Catalyst-free, high selective CO₂ reduction in strong acid without alkali cations by mechanical energy-induced triboelectric plasma-electrolytic system

Hui Hu,^a Nannan Liu,^a Qinglong Ru,^a Wei Jiang,^a Yongcui Yang,^a Kailan Ma,^a Lixiang Meng,^a
Zuliang Du,^a Bao Zhang^{*a} and Gang Cheng^{*a}

^a Key Lab for Special Functional Materials, Ministry of Education, National & Local Joint Engineering Research Center for High-efficiency Display and Lighting Technology, School of Nanoscience and Materials Engineering, and Collaborative Innovation Center of Nano Functional Materials and Applications, Henan University, Kaifeng, 475004, China

*Corresponding author: zhangbao@henu.edu.cn and chenggang@henu.edu.cn.

Table of Contents

Part I. Supplementary experimental section.....	S3
1. Materials.....	S3
2. Fabrication of TENG	S3
3. Mechanical energy-driven hybrid triboelectric plasma electrolytic CO₂RR system 	S4
4. Split cell experiment	S5
5. Calculations of activity, selectivity, and energy efficiency	S6
6. Control experiments	S7
7. Long-term stability test.....	S8
Part II. Supplementary Figs. S1-S16 & Table S1.....	S9
Part III. Supplementary references	S27

Part I. Supplementary experimental section

1. Materials

H₂SO₄ and HCl were obtained from Luoyang Haohua Chemical Reagent Co., Ltd. (Luoyang, China). CH₃COOH, H₃PO₄, and HCOOH were obtained from Tianjin Fuyu Fine Chemical Co., Ltd. (Tianjin, China). HNO₃, Dimethyl sulfoxide (DMSO), and HClO₄ were obtained from Chengdu Chron Chemical Co., Ltd. (Chengdu, China). CF₃SO₃H, C₂D₄O₂, D₃PO₄, and D₂SO₄ were obtained from J&K Scientific (Beijing, China). Hexadecyl trimethyl ammonium bromide (CTAB) was obtained from Tianjin Kemiou Chemical Reagent Co., Ltd. (Tianjin, China). 5,5-dimethyl-1-pyrroline N-oxide (DMPO) was obtained from Shanghai Titan Technology Co., Ltd. (Shanghai, China). Water was purchased from Hangzhou Wahaha Group Co., Ltd. (Hangzhou, China). Ar, He, and CO₂ gas were supplied from Henan Yuanzheng Special Gas Co., Ltd. (Zhengzhou, China).

2. Fabrication of TENG

In this study, a TENG was chosen as the driving force to generate triboelectric plasma. The TENG was composed of three components: electrodes, a dielectric layer, and a triboelectric layer. The electrode layer was constructed by an 80.0 mm-thick copper film, which stuck on a 0.5 cm-thick printed circuit board. Moreover, the electrode layer adhered to a 40 mm-diameter and 4.0 mm-thick acrylic plate to form the stator. The copper electrode was divided into quadrants. Each sector occupied one-quarter of the acrylic plate. The distance between copper electrodes in adjacent sectors

was 1.0 cm. The two fan-shaped alternating copper electrodes were connected via copper wires. A 40 mm-diameter and 0.08 mm-thick polytetrafluoroethylene (PTFE) was employed as the dielectric layer, which also stuck on the Cu film. Rabbit fur was used as the triboelectric layer, divided into two equal-sized fan-shaped regions, the same size as the fan-shaped copper electrodes. The rabbit fur was alternately pasted on a 40 mm-diameter and 6.0 mm-thick circular acrylic plate substrate to form the rotor. Then, the formed rotor was connected to the generator shaft via a flange. The TENG was connected to the rectifier bridge to supply pulsed current and voltage.

3. Mechanical energy-driven hybrid triboelectric plasma electrolytic CO₂RR system

In this study, the hybrid triboelectric plasma electrolytic CO₂RR device enabled by mechanical energy was composed of four components, namely the upper and lower glass reactors (with outer and inner diameters of 2.0 and 1.8 cm, respectively) and two electrodes (tungsten needles with a curvature radius of 5 μm and platinum wire electrodes with a diameter of 0.5 mm). The tungsten needle was in the nozzle of the upper glass reactor and was connected to the negative polarity of the rectifier bridge (the nozzle's outer diameter was 9 mm). The platinum wire was fixed at the bottom of the lower glass reactor and connected to the positive polarity of the rectifier bridge, while electrolyte solution was added to the lower glass reactor. A hose with an inner diameter of 0.8 mm and an outer diameter of 4 mm was connected to the gas inlet of the upper reactor, through which the CO₂ flow controlled by the flow controller (Beijing Seven Starflight Electronic Co., Ltd) was purged into the glass reactor. The products

first passed through a drying tube equipped with a 13X molecular sieve and changed color silica gel to remove the excessive water molecules in the gas outlet; Meanwhile, the concentrations of CO and H₂ were detected using a gas chromatograph (Agilent 7890B, USA) with a thermal conductivity detector and a flame ionization detector. The resulting gas product was injected into the gas chromatograph every 9 minutes. The gas chromatograph employed Ar/He (predominantly Ar) as the carrier gas, and the column temperature was 90 °C. The liquid products of CO₂RR were examined by proton nuclear magnetic resonance spectroscopy (400 MHz).

Prior to the reaction, CO₂ was purged through the upper glass reactor for 0.5 h to eliminate residual air from the hybrid triboelectric plasma electrolytic system. The mechanical energy-driven hybrid triboelectric plasma electrolytic CO₂RR experiments were conducted under the conditions of a TENG rotational speed of 180 rpm, CO₂ flow rate of 10 mL min⁻¹, negative polarity, a discharge distance of 1.5 mm, 0.05 mol L⁻¹ H₂SO₄ solution, at room temperature and atmospheric pressure. The effects of factors such as the rotational speed of the TENG, the flow rate of CO₂ gas, discharge polarity, discharge distance, electrolyte, and concentration of electrolyte on the CO₂RR performance were investigated.

4. Split cell experiment

In the H-type split cell, the platinum wire anode and the triboelectric plasma cathode were placed in two separate chambers, respectively. A proton exchange membrane was applied at the junction of the split H-cell. In addition, at the same TENG rotational speed, the reaction conditions of the single cell and the split cell remained

the same. The products of the two chambers of the division cell were detected independently. The gas chromatograph was used to detect CO and H₂ concentration with Ar as the carrier gas and CO and O₂ concentration with He as the carrier gas.

5. Calculations of activity, selectivity, and energy efficiency

The calculation formula of the CO/O₂/H₂ evolution rate was as follows:

$$r_{CO} = C_{CO} \times Q \times 60 \quad (\text{Equation 1})$$

$$r_{H_2} = C_{H_2} \times Q \times 60 \quad (\text{Equation 2})$$

$$r_{O_2} = C_{O_2} \times Q \times 60 \quad (\text{Equation 3})$$

where the C_{CO} , C_{H_2} , and C_{O_2} is the concentration of CO, H₂, and O₂ (μmol L⁻¹), respectively, and Q is the flow rate of the CO₂ gas (L min⁻¹).

The calculation formula of the CO selectivity was as follows:

$$S_{CO} = \frac{r_{CO}}{r_{CO} + r_{H_2}} \quad (\text{Equation 4})$$

The discharge characteristics of the hybrid triboelectric plasma electrolysis system were monitored using a dual-channel electrometer configured for simultaneous voltage and current measurements. One channel monitored the discharge current directly. The other channel obtained the discharge signals by adjusting an appropriate matched resistor that established a zero baseline reference. The discharge voltage was subsequently obtained by multiplying the known resistance value by the measured discharge current. All electrical signals were recorded at high temporal resolution using a LabView-controlled data acquisition system operating at 2 M sampling rate.

The calculation formula of electrical energy cost of triboelectric plasma was

calculated as:

$$P_{ave} = \frac{\int_0^t V \times I dt}{t} \quad (\text{Equation 5)}$$

5)

where V is the calculated voltage (V), I is the obtained current (A), and t is the reaction time (s).

The calculation formula of conversion efficiency of electrical to chemical energy

($\eta_{ele-chem}$) was calculated as follows :

$$\eta_{ele-co} = \frac{r_{CO} \times \Delta_r H^\theta(CO)}{P_{ave} \times 3600} \quad (\text{Equation 5})$$

5)

$$\eta_{ele-H_2} = \frac{r_{H_2} \times \Delta_r H^\theta(H_2)}{P_{ave} \times 3600} \quad (\text{Equation 6})$$

6)

where the $\Delta_r H^\theta(CO)$, $\Delta_r H^\theta(H_2)$ is the enthalpy change of CO₂ splitting to CO or H₂O splitting to H₂ (279.8, 285.8 kJ mol⁻¹).

6. Control experiments

We conducted a series of control experiments to verify the CO/H₂ formation mechanism. The specific experimental methods were as follows: (i) CO₂ was introduced simultaneously into both the upper and lower glass reactors under non-plasma conditions. Reaction conditions: no external TENG, CO₂ gas flow rate of 10 mL min⁻¹ as the supply gas of triboelectric plasma and CO₂ gas flow rate of 5 mL min⁻¹ as the purge gas passing through H₂SO₄ solution, negative polarity, discharge distance

of 1.5 mm, 0.05 mol L⁻¹ H₂SO₄ solution, room temperature, and atmospheric pressure.

(ii) Ar was utilized as the triboelectric plasma supply gas, which flows into the glass sidearm of the upper reactor. Moreover, Ar was also the purge gas passing through H₂SO₄ solution through the lower glass reactor. Reaction conditions: TENG rotational speed of 180 rpm, Ar gas flow rate of 10 mL min⁻¹ as the supply gas of the triboelectric plasma and Ar gas flow rate of 5 mL min⁻¹ as the purge gas passing through the H₂SO₄ solution, negative polarity, discharge distance of 1.5 mm, 0.05 mol L⁻¹ H₂SO₄ solution, room temperature, and atmospheric pressure; (iii) Ar was employed as the triboelectric plasma supply gas, which flows into the glass sidearm of the upper reactor, and CO₂ as the purge gas, which flows into H₂SO₄ solution through the lower glass reactor. Reaction conditions: TENG rotational speed of 180 rpm, Ar gas flow rate of 10 mL min⁻¹ as the supply gas of the triboelectric plasma and CO₂ gas flow rate of 5 mL min⁻¹ as the purge gas passing through H₂SO₄ solution, negative polarity, discharge distance of 1.5 mm, 0.05 mol L⁻¹ H₂SO₄ solution, room temperature, and atmospheric pressure.

(iv) CO₂ was adopted as both the triboelectric plasma supply gas in the upper glass reactor and purge gas in the lower glass reactor. Reaction conditions: TENG rotational speed of 180 rpm, CO₂ gas flow rate of 10 mL min⁻¹, negative polarity, discharge distance of 1.5 mm, 0.05 mol L⁻¹ H₂SO₄ solution, room temperature, and atmospheric pressure.

7. Long-term stability test

During the stability test, we also observed that, in each operation cycle the obtained CO evolution rate (r_{CO}) remained consistent. The duration of the experiment

was 120 h, and 0.05 mol L⁻¹ H₂SO₄ solution was reloaded each 4 h. The mechanical energy-driven hybrid triboelectric plasma electrolytic CO₂RR experiments were conducted under the conditions of a TENG rotational speed of 180 rpm, CO₂ flow rate of 10 mL min⁻¹, negative polarity, a discharge distance of 1.5 mm, 0.05 mol L⁻¹ H₂SO₄ solution, at room temperature and atmospheric pressure.

Part II. Supplementary Figs. S1-S16 & Table S1

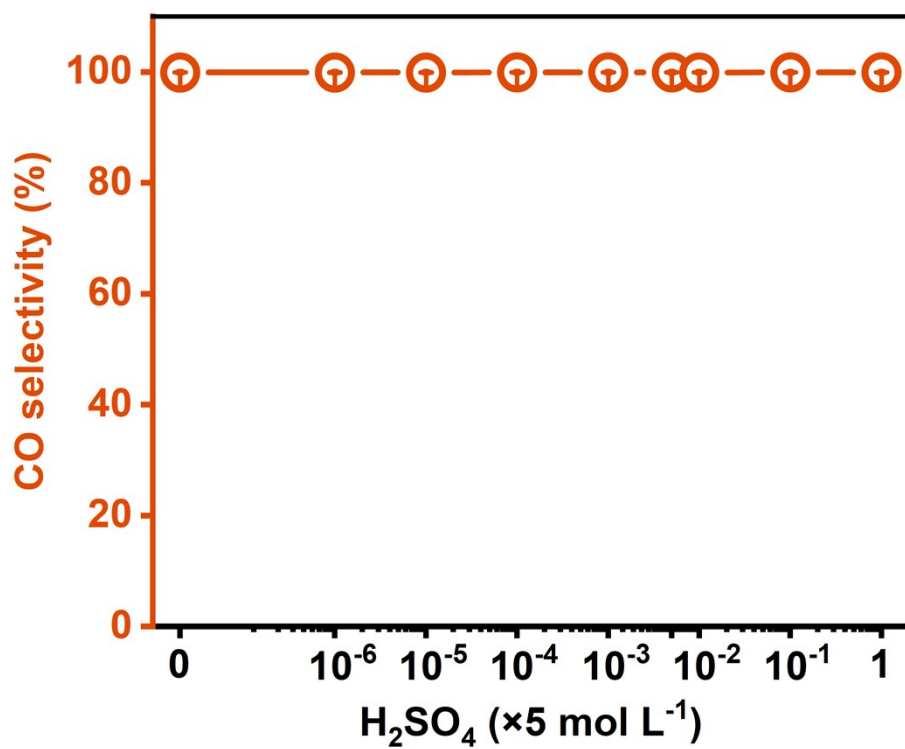


Fig. S1 CO selectivity as a function of H₂SO₄ concentration. Reaction conditions: TENG rotational speed of 180 rpm, CO₂ gas flow rate of 10 mL min⁻¹, negative polarity, discharge distance of 1.5 mm, normal temperature, and atmospheric pressure.

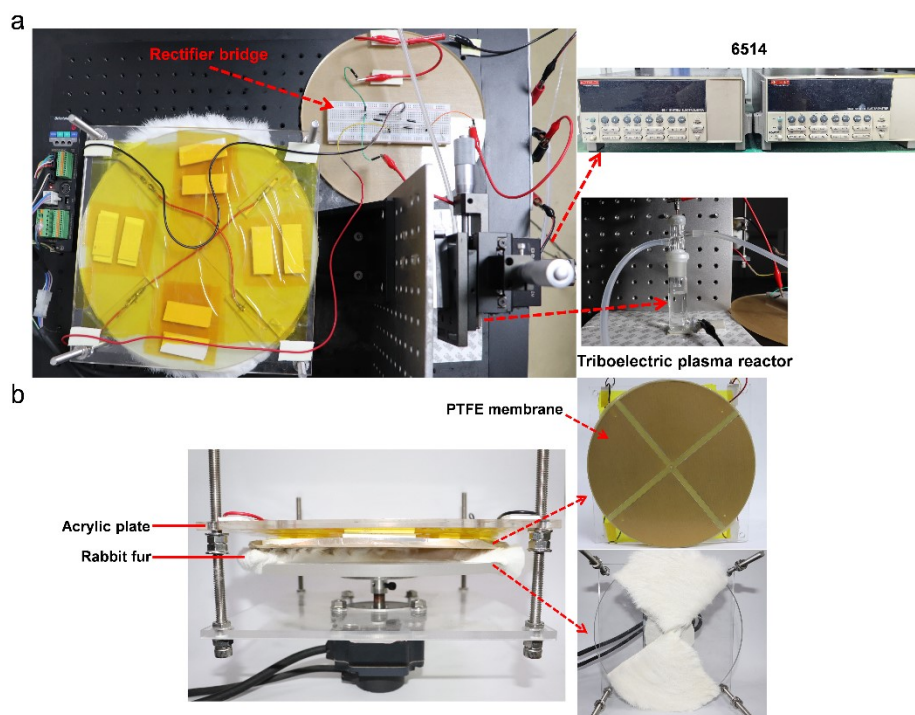


Fig. S2 Mechanical energy-induced triboelectric plasma-electrolytic carbon dioxide reduction system. (a) Schematic of the experimental device. (b) Separated triboelectric layers and contacting triboelectric layers of the TENG.

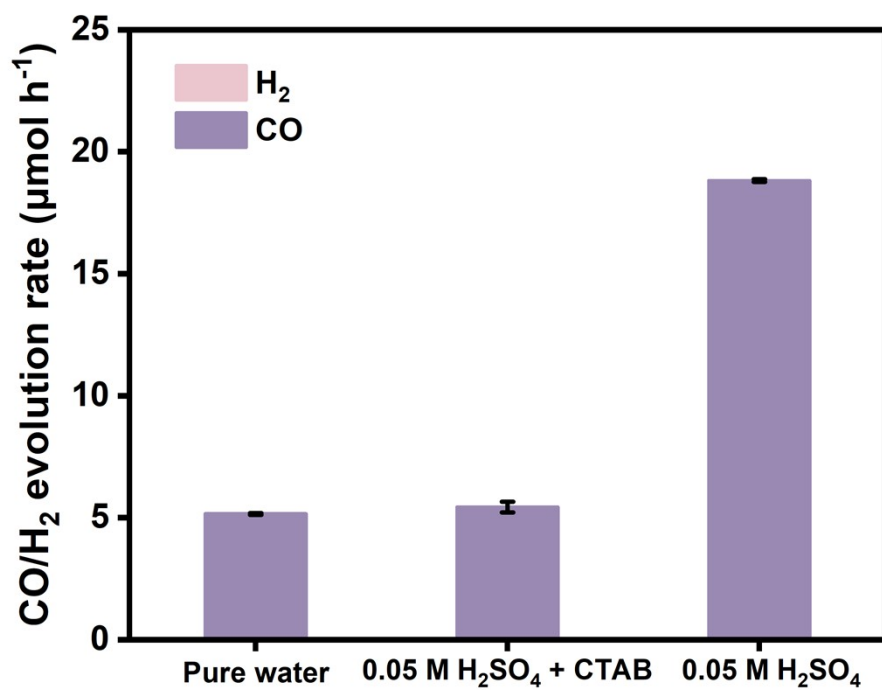


Fig. S3 CO evolution rate (r_{CO}) of pure water, 0.05 mol L⁻¹ H₂SO₄ solution + CTAB (30 mg), and 0.05 mol L⁻¹ H₂SO₄ solution. Reaction conditions: TENG rotational speed of 180 rpm, CO₂ gas flow rate of 10 mL min⁻¹, negative polarity, discharge distance of 1.5 mm, normal temperature, and atmospheric pressure.

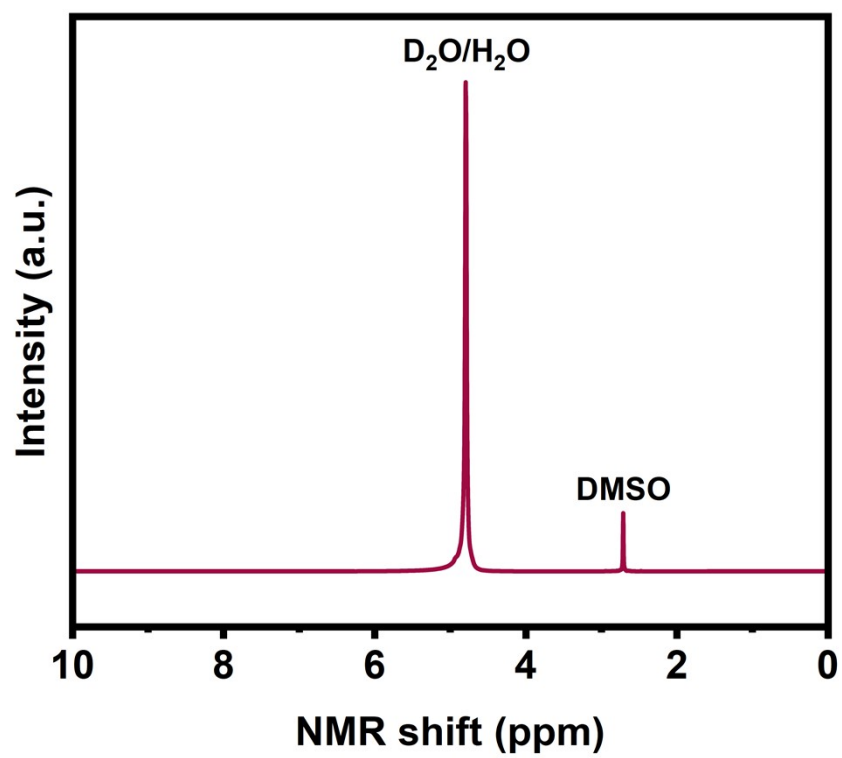


Fig. S4 ¹H NMR spectra of liquid products obtained after 4 h.

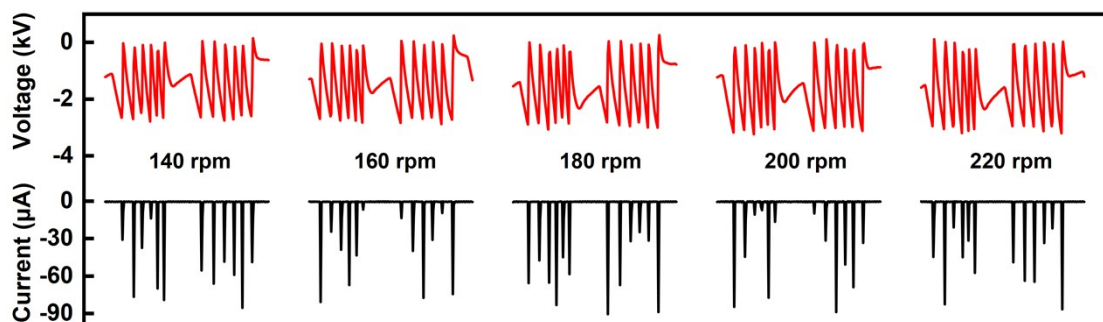


Fig. S5 Discharge voltage and current as a function of TENG rotational speed. Reaction conditions: CO₂ gas flow rate of 10 mL min⁻¹, negative polarity, discharge distance of 1.5 mm, 0.05 mol L⁻¹ H₂SO₄ solution, normal temperature, and atmospheric pressure.

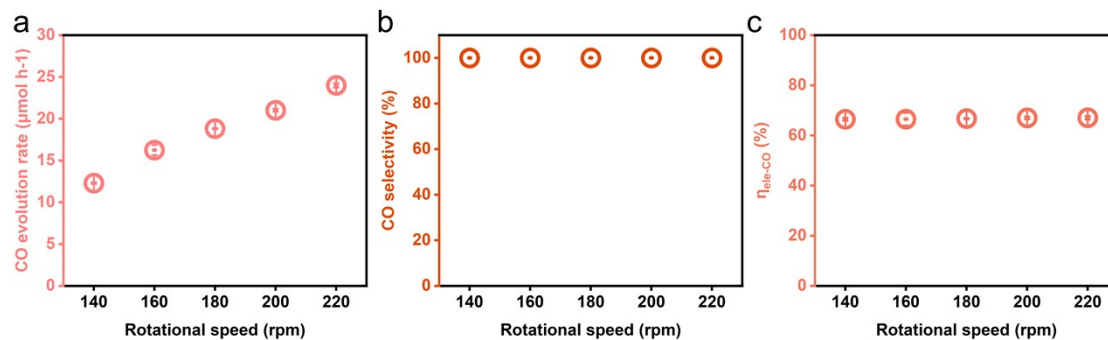


Fig. S6 (a-c) CO evolution rate (r_{CO}), CO selectivity, and electrical to chemical energy efficiency (η_{ele-CO}) as a function of TENG rotational speed. Reaction conditions: CO_2 gas flow rate of 10 mL min^{-1} , negative polarity, discharge distance of 1.5 mm, 0.05 mol L^{-1} H_2SO_4 solution, normal temperature, and atmospheric pressure.

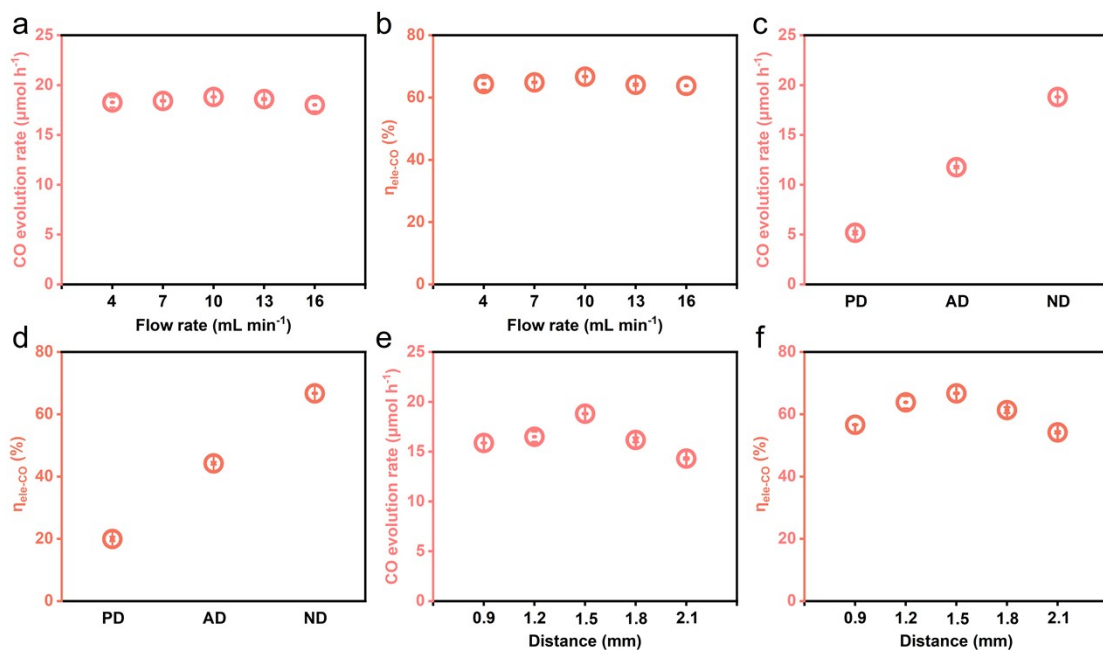


Fig. S7 Influence of gas-phase triboelectric plasma. (a-b) CO evolution rate (r_{CO}) and electrical to chemical energy efficiency ($\eta_{\text{ele-CO}}$) under different CO_2 gas flow rates. (c-d) CO evolution rate (r_{CO}) and electrical to chemical energy efficiency ($\eta_{\text{ele-CO}}$) under different discharge polarities. (e-f) CO evolution rate (r_{CO}) and electrical to chemical energy efficiency ($\eta_{\text{ele-CO}}$) at different discharge distances. Reaction conditions: TENG rotational speed of 180 rpm, $0.05 \text{ mol L}^{-1} \text{ H}_2\text{SO}_4$ solution, normal temperature, and atmospheric pressure.

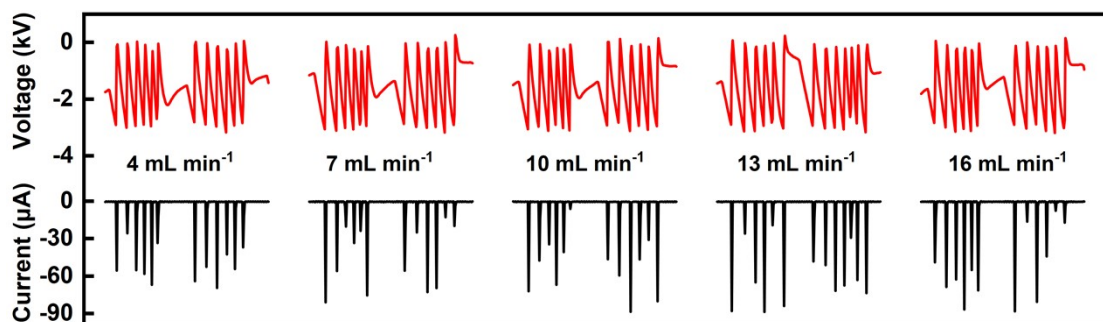


Fig. S8 Discharge voltage and current as a function of CO₂ gas flow rate. Reaction conditions: TENG rotational speed of 180 rpm, negative polarity, discharge distance of 1.5 mm, 0.05 mol L⁻¹ H₂SO₄ solution, normal temperature, and atmospheric pressure.

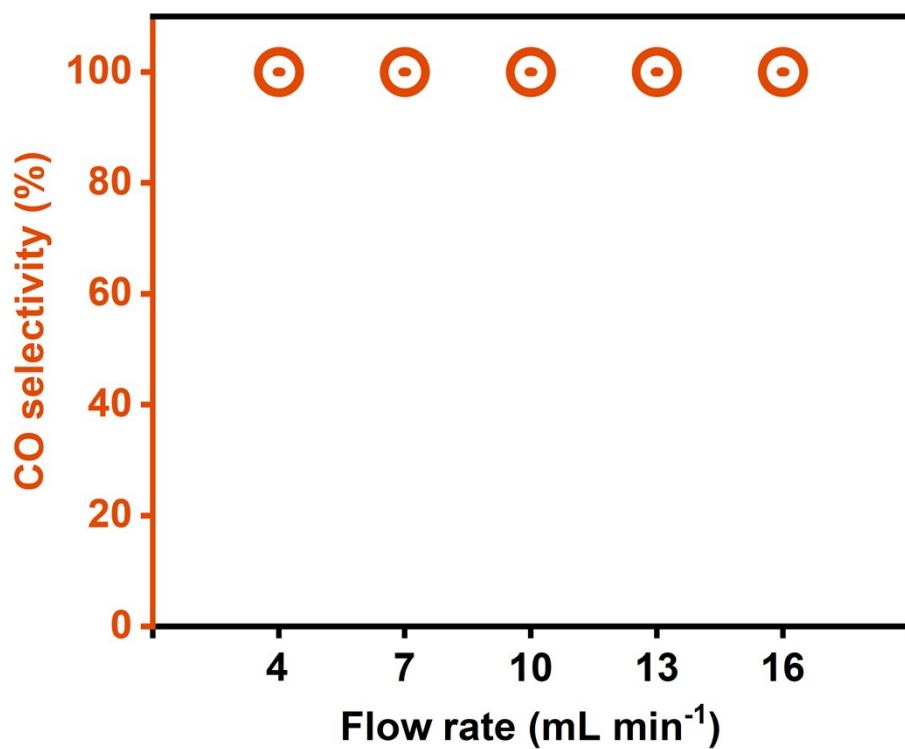


Fig. S9 CO selectivity as a function of CO₂ gas flow rate. Reaction conditions: TENG rotational speed of 180 rpm, negative polarity, discharge distance of 1.5 mm, 0.05 mol L⁻¹ H₂SO₄ solution, normal temperature, and atmospheric pressure.

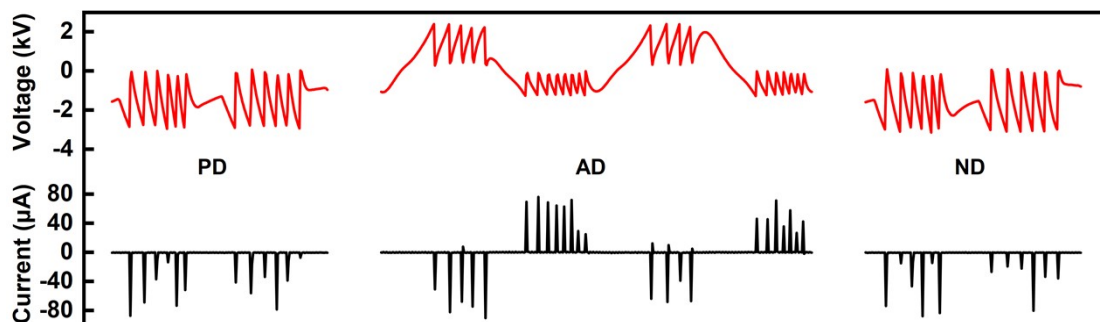


Fig. S10 Discharge voltage and current as a function of discharge polarities. PD = positive discharge, AD = alternative discharge, ND = negative discharge. Reaction conditions: TENG rotational speed of 180 rpm, CO₂ gas flow rate of 10 mL min⁻¹, discharge distance of 1.5 mm, 0.05 mol L⁻¹ H₂SO₄ solution, normal temperature, and atmospheric pressure. Note: For AD condition, the tungsten needle electrode and platinum wire electrode were directly connected to the output terminals of the TENG. For PD condition, the tungsten needle is connected to the positive terminal of the rectifier bridge, while the platinum wire is connected to the negative terminal. For ND condition, the tungsten needle is connected to the negative terminal of the rectifier bridge, and the platinum wire is connected to the positive output terminal.

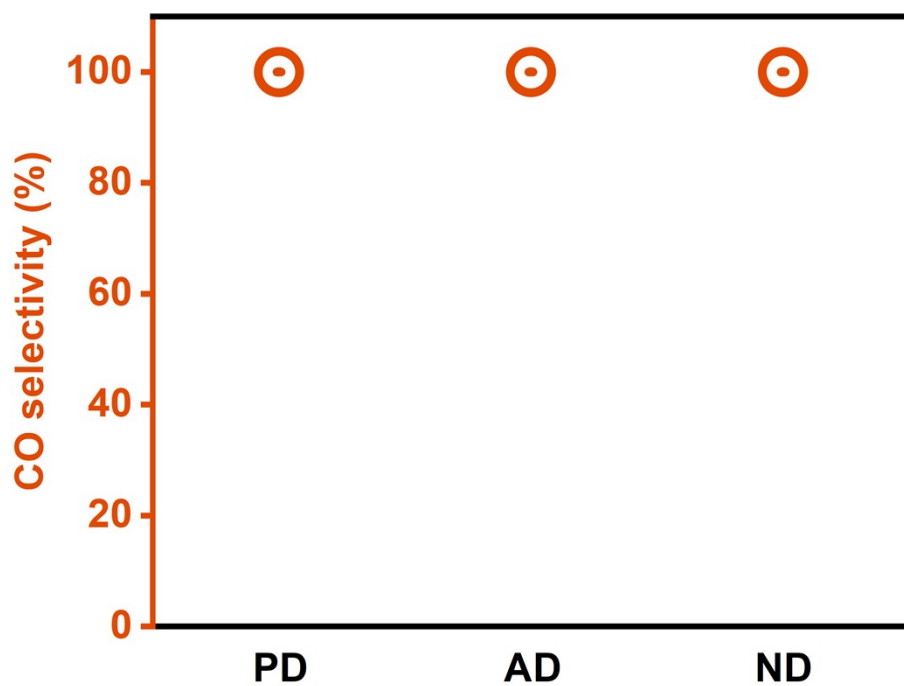


Fig. S11 CO selectivity as a function of discharge polarities. Reaction conditions: TENG rotational speed of 180 rpm, CO₂ gas flow rate of 10 mL min⁻¹, discharge distance of 1.5 mm, 0.05 mol L⁻¹ H₂SO₄ solution, normal temperature, and atmospheric pressure.

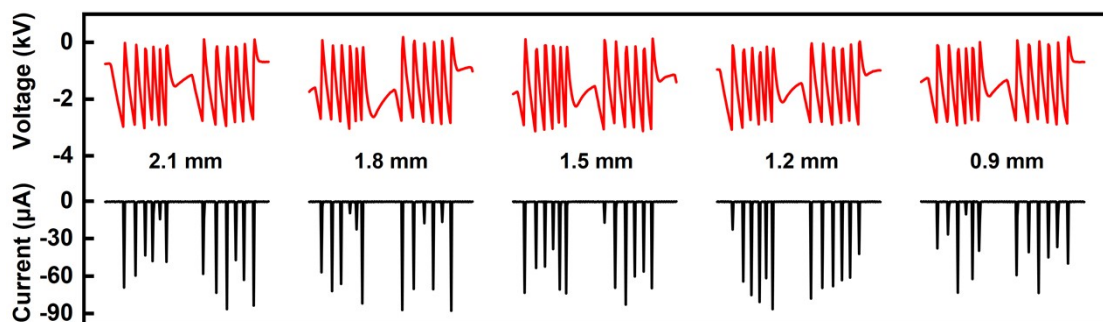


Fig. S12 Discharge voltage and current as a function of discharge distances. Reaction conditions: TENG rotational speed of 180 rpm, CO₂ gas flow rate of 10 mL min⁻¹, negative polarity, 0.05 mol L⁻¹ H₂SO₄ solution, normal temperature, and atmospheric pressure.

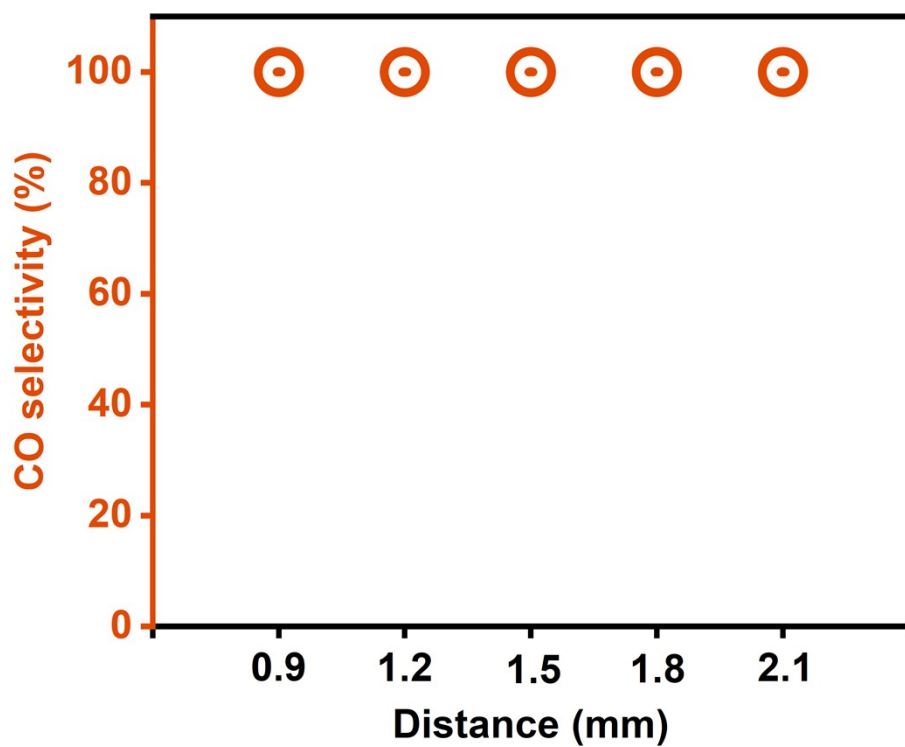


Fig. S13 CO selectivity as a function of discharge distances. Reaction conditions: TENG rotational speed of 180 rpm, CO₂ gas flow rate of 10 mL min⁻¹, negative polarity, 0.05 mol L⁻¹ H₂SO₄ solution, normal temperature, and atmospheric pressure.

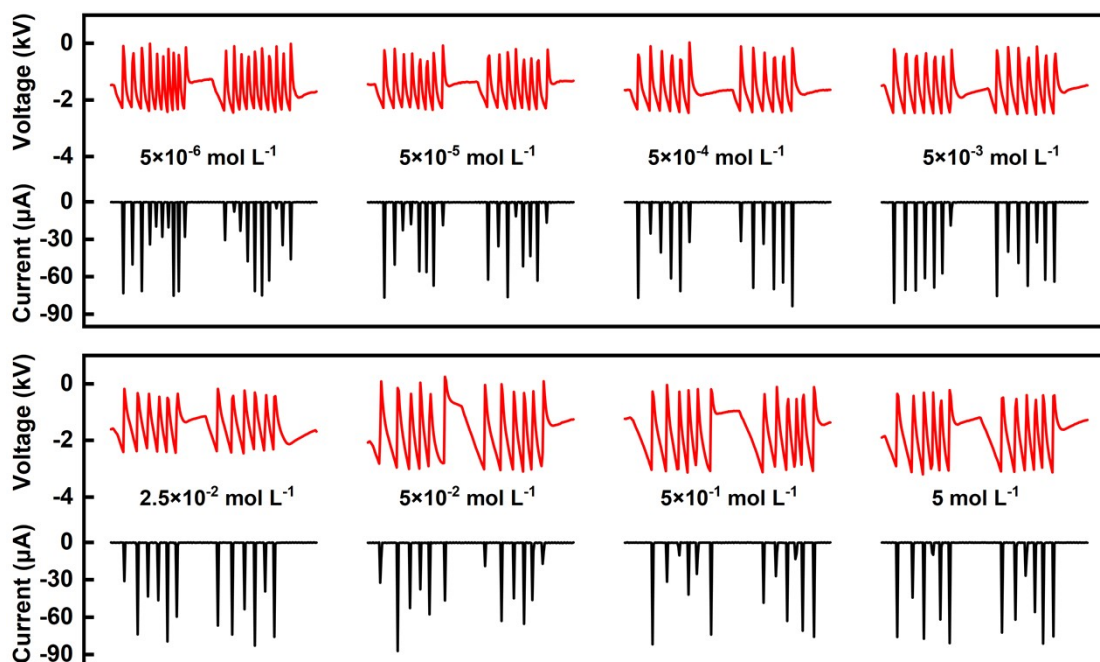


Fig. S14 Discharge voltage and current as a function of H_2SO_4 concentration. Reaction conditions: TENG rotational speed of 180 rpm, CO_2 gas flow rate of 10 mL min^{-1} , negative polarity, discharge distance of 1.5 mm, normal temperature, and atmospheric pressure.

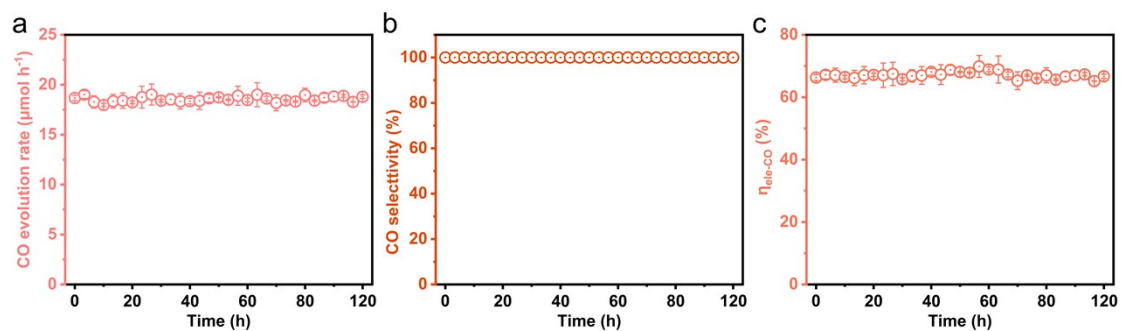


Fig. S15 Long-term stability for 120 hours. (a-c) CO evolution rate (r_{CO}), CO selectivity, and electrical to chemical energy efficiency ($\eta_{\text{ele-CO}}$) of $0.05 \text{ mol L}^{-1} \text{ H}_2\text{SO}_4$ solution. Reaction conditions: TENG rotational speed of 180 rpm, CO_2 gas flow rate of 10 mL min^{-1} , negative polarity, discharge distance of 1.5 mm, normal temperature, and atmospheric pressure.

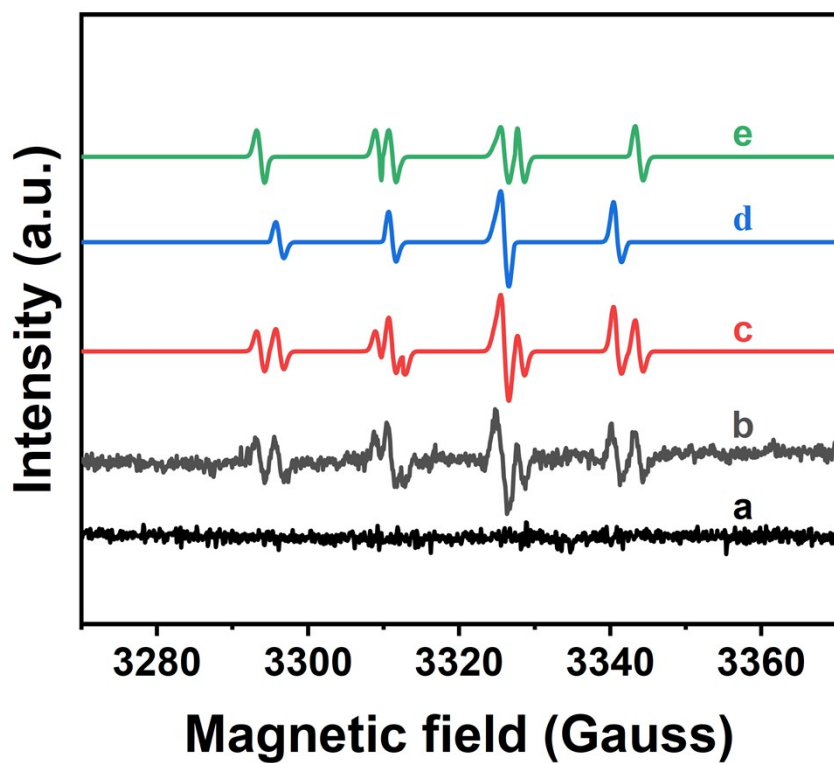


Fig. S16 Electron paramagnetic resonance (EPR) results of hybrid triboelectric plasma electrochemical system under acidic conditions. (a) EPR signal without triboelectric plasma; (b) EPR signal under triboelectric plasma; (c) Sum of simulated EPR signals of DMPO-OH and DMPO-CO₂⁻; (d) Simulated EPR signal of DMPO-OH; (e) Simulated EPR signal of DMPO-CO₂⁻.

Supplementary Table S1. Comparison of different methods for electrolytic CO₂RR in acids.

Reference	Reaction conditions	Catalyst	Product selectivity	Production rate	Faraday efficiency (FE) / Energy efficiency (EE)
1	0.1 M H ₂ SO ₄ + 0.4 M K ₂ SO ₄	Au/C	-	-	CO FE of 91%, H ₂ FE of < 10% EE of 28%
2	0.01 M H ₂ SO ₄	Cationic-group-functionalized electrocatalysts	-	-	CO ₂ to C ₂ ⁺ , H ₂ FE of < 10.0% Multicarbon products FE of 83.7 ± 1.4%, H ₂ FE of 6.3%
3	0.05 M H ₂ SO ₄ + 3 M KCl	ER-CuNS	-	-	CO FE of ~100%, H ₂ FE of < 10%
4	0.05 M H ₂ SO ₄ + 0.1 M KCl	CoTAAPc@CN T-12	-	-	C ₂ H ₄ FE of 61%, C ₂ ⁺ FE of 82%, H ₂ FE of < 10%
5	0.5 M H ₃ PO ₄ and 0.5 M KH ₂ PO ₄ with 2.5 M KCl	CoPc@HC and Cu nanocatalyst	-	-	C ₂ ⁺ FE of 86.2%, H ₂ FE of 7.2%
6	0.05 M H ₂ SO ₄ + 3 M KCl	La-Cu HS catalyst	-	-	HCOOH FE of > 90%, H ₂ FE of < 10%
7	0.05 M H ₂ SO ₄ + 3 M KCl	SiC-Nafion TM /SnBi/P TFE	-	-	

8	0.05 M H ₂ SO ₄ + 3 M KCl	Bi nanosheets	-	-	HCOOH FE of 92.2%, H ₂ FE of < 10% CO FE of 85%, H ₂ FE of < 10%
9	0.01 M H ₂ SO ₄	PDDA-GO to modify Ag catalysts	-	-	H ₂ FE of < 10%
10	0.1 M H ₂ SO ₄ + 0.13 M K ₂ SO ₄	Ni-SAC-CNTs	CO selectivity to exceed 90%	-	H ₂ FE of < 10%
11	0.5 M H ₂ SO ₄ + 3 M KCl	Cu NNS	-	-	C ₂ ⁺ FE of 90.69 ± 2.15%, H ₂ FE of < 10%
12	0.1 M H ₂ SO ₄	c-PDDA decorated Ag NPs	-	-	CO FE of 95 ± 3%, H ₂ FE of < 3% ± 1%
This work	0-5 M H ₂ SO ₄	-	nearly 100% CO	18.8 μmol h ⁻¹	$\eta_{ele-chem}$ of 66.7%

Note: M=mol L⁻¹, FE=Faradaic Efficiency

Part III. Supplementary references

- 1 J. Gu, S. Liu, W. Y. Ni, W. H. Ren, S. Haussener and X. L. Hu, *Nat. Catal.*, 2022, **5**, 268-276.
- 2 M. Fan, J. E. Huang, R. K. Miao, Y. Mao, P. Ou, F. Li, X.-Y. Li, Y. Cao, Z. Zhang, J. Zhang, Y. Yan, A. Ozden, W. Ni, Y. Wang, Y. Zhao, Z. Chen, B. Khatir, C. P. O'Brien, Y. Xu, Y. C. Xiao, G. I. N. Waterhouse, K. Golovin, Z. Wang, E. H. Sargent and D. Sinton, *Nat. Catal.*, 2023, **6**, 763-772.
- 3 Z. Ma, Z. Yang, W. Lai, Q. Wang, Y. Qiao, H. Tao, C. Lian, M. Liu, C. Ma, A. Pan and H. Huang, *Nat. Commun.*, 2022, **13**, 7596.
- 4 Q. Zhang, C. B. Musgrave, Y. Song, J. Su, L. Huang, L. Cheng, G. Li, Y. Liu, Y. Xin, Q. Hu, G. Ye, H. Shen, X. Wang, B. Z. Tang, W. A. Goddard and R. Ye, *Nat. Synth.*, 2024, **3**, 1231-1242.
- 5 Y. Chen, X.-Y. Li, Z. Chen, A. Ozden, J. E. Huang, P. Ou, J. Dong, J. Zhang, C. Tian, B.-H. Lee, X. Wang, S. Liu, Q. Qu, S. Wang, Y. Xu, R. K. Miao, Y. Zhao, Y. Liu, C. Qiu, J. Abed, H. Liu, H. Shin, D. Wang, Y. Li, D. Sinton and E. H. Sargent, *Nat. Nanotechnol.*, 2023, **19**, 311-318.
- 6 J. Feng, L. Wu, X. Song, L. Zhang, S. Jia, X. Ma, X. Tan, X. Kang, Q. Zhu, X. Sun and B. Han, *Nat. Commun.*, 2024, **15**, 4821.
- 7 L. Li, Z. Liu, X. Yu and M. Zhong, *Angew. Chem. Int. Ed.*, 2023, **62**, e202300226.
- 8 Y. Qiao, W. Lai, K. Huang, T. Yu, Q. Wang, L. Gao, Z. Yang, Z. Ma, T. Sun, M. Liu, C. Lian and H. Huang, *ACS Catal.*, 2022, **12**, 2357-2364.
- 9 J. Fan, B. Pan, J. Wu, C. Shao, Z. Wen, Y. Yan, Y. Wang and Y. Li, *Angew. Chem. Int. Ed.*, 2024, **63**, e202317828.
- 10 J. Kim, T. H. Ha, J. Kim, G. H. Jeong, S. O. Kim, W. Chung, K. Roh, J. H. Lee and J. Oh, *Appl. Catal. B, Environ.*, 2023, **339**, 123160.
- 11 X. Zi, Y. Zhou, L. Zhu, Q. Chen, Y. Tan, X. Wang, M. Sayed, E. Pensa, R. A. Geioushy, K. Liu, J. Fu, E. Cortés and M. Liu, *Angew. Chem. Int. Ed.*, 2023, **62**, e202309351.
- 12 H.-G. Qin, Y.-F. Du, Y.-Y. Bai, F.-Z. Li, X. Yue, H. Wang, J.-Z. Peng and J. Gu, *Nat. Commun.*, 2023, **14**, 5640.